Soft Matter

PAPER

View Article Online
View Journal | View Issue

Cite this: *Soft Matter*, 2020, **16**, 4155

High antisite defect concentrations in hard-sphere colloidal Laves phases†

Berend van der Meer, [a] Frank Smallenburg, [b] Marjolein Dijkstra[a] and Laura Filion *[a]

Received 25th February 2020,
Accepted 1st April 2020

DOI: 10.1039/d0sm00335b

rsc.li/soft-matter-journal

Binary mixtures of hard spheres can spontaneously self-assemble into binary crystals. Computer simulations have been especially useful in mapping out the phase behaviour of these mixtures, under the assumption that the stoichiometry of the binary crystal is ideal. Here we show that for a size ratio of $q = 0.82$ this assumption is not valid near the coexistence region between the fluid and the stable binary crystal, the $MgZn_2$ Laves phase. Instead we find a surprisingly high number of antisite defects: up to 2% of the large spheres are replaced by small spheres in equilibrium. We demonstrate that the defect concentration can be estimated using simple approximations, providing an easy way to identify systems where antisite defects play an important role. Our results shed new light on the self-assembly of colloidal Laves phases, and demonstrate the importance of antisite defects in binary crystals.

1 Introduction

In equilibrium, all crystals are marred by a small concentration of point defects, such as vacancies and interstitials. These defects strongly affect the optical and mechanical properties of crystalline materials, and are the main agents for transport in crystals. In systems of more than one component, in addition to vacancies and interstitials, new forms of point defects arise: a lattice site of one species can be filled by a particle of another species, creating a so-called "antisite" defect.[1] Such defects are most likely to occur when two species of particle in the crystal have very similar interactions, such that one easily "fits" on a mismatched lattice site. On the atomic scale, antisite defects often occur in alloys, and play an important role in *e.g.* the electronic properties of semiconductors such as GaAs.[2] However, when predicting colloidal phase behavior, antisite defects have, until now, been ignored.[3–8] This is particularly surprising since colloidal interactions, which are typically short-ranged and weak in comparison to the thermal energy scale, are ideal for the formation of antisite defects.

Here, we explore the effect of antisite defects on the phase diagram of a binary hard-sphere mixture. Binary hard-sphere mixtures are perhaps the simplest possible model for studying binary crystal structures, and have been instrumental in understanding the phase behavior of colloidal systems.[3–31] The equilibrium phase diagrams of binary hard-sphere mixtures for various size ratios have been extensively explored using simulations,[3–8,11,22,31] revealing a number of stable binary crystal structures. However, even for this classical colloidal system, antisite defects have not been considered. Here, we focus our attention on binary hard spheres with a size ratio of $q = \frac{\sigma_S}{\sigma_L} = 0.82$, where $\sigma_{S(L)}$ is the diameter of the small (large) particles. For this size ratio, previous studies have concluded that the phase diagram contains a binary fluid phase, single-component face-centered-cubic (FCC) crystals of both the large and small particles, and a binary crystal phase. The stable binary crystal is the $MgZn_2$ Laves phase, with two other Laves phases, $MgCu_2$ and $MgNi_2$ closely competing.[8] Note that these phases are very similar and differ by the stacking of the large particles. As the $MgZn_2$ phase has been shown to be the most stable one, we will focus on it in this paper, and in the following use the terms $MgZn_2$ Laves phase and Laves phase interchangeably.

Of all stable binary hard-sphere crystal structures, $MgZn_2$ occurs for size ratios closest to 1, suggesting that switching out a particle in the crystal with one of the opposite species carries a relatively low free-energy cost. Hence, this structure is a prime candidate for exploring the effect of antisite defects on equilibrium phase behavior. Moreover, colloidal Laves phases have drawn considerable attention, due to the interesting photonic properties of the sublattices of the $MgCu_2$ phase.[7,32] Such properties could be affected by the presence of defects.

In this study, we use Monte Carlo simulations and thermodynamic integration to calculate the free energy of FCC and $MgZn_2$ hard-sphere crystals as a function of the antisite defect

[a] *Soft Condensed Matter, Debye Institute for Nanomaterials Science, Utrecht University, Princetonplein 5, 3584 CC Utrecht, The Netherlands. E-mail: L.C.Filion@uu.nl*
[b] *Université Paris-Saclay, CNRS, Laboratoire de Physique des Solides, 91405 Orsay, France*

† Electronic supplementary information (ESI) available. See DOI: 10.1039/d0sm00335b

concentration. Combining this free energy with that of the fluid, we predict the equilibrium phase behavior. The new phase diagram differs significantly from the phase diagram calculated without taking defects into account:[8] while in the defect-free phase diagram, the Laves phase was only stable at the ideal composition, in the new phase diagram, the Laves phase covers a range of compositions, all of which correspond to a higher fraction of small particles than in the perfect crystal. This correction arises from a significant concentration of antisite defects, with up to 2% of the large-particle lattice sites occupied by a small particle. This defect concentration is orders of magnitude higher than the vacancy and interstitial defect concentrations found in monodisperse hard-sphere crystals.[33,34] Finally, we demonstrate that the defect concentration can be estimated using simple approximations, providing a fast and easy way to identify systems where antisite defects play an important role.

2 Free energy of antisite defects

We begin by considering the impact of antisite defects on the free energy of the $MgZn_2$ hard-sphere crystal. In the ideal $MgZn_2$ crystal (see Fig. 1(a)), there is one large particle (denoted L) for every two small particles (S), and each particle is on a lattice site corresponding to its own species. In principle, however, the free energy of the crystal will be minimized when there are a finite number of local mistakes, including vacancies, interstitials and antisite defects. Previous studies of hard-sphere systems have found (at least in the case of single-component crystals), that the equilibrium concentration of vacancies and interstitials is very small. Specifically, for hard spheres near melting, the concentration of vacancies and interstitials is predicted to be 10^{-4} and 10^{-8}, respectively.[33–35] Here, we focus on the possibility of antisite defects. Using Kröger–Vink notation, we denote a small particle occupying a large-particle lattice site as S_L and a large particle occupying a small-particle lattice site as L_S. Fig. 1(b) and (c) shows illustrations of both types of defects.

We now consider the Helmholtz free energy of a binary crystal with M lattice sites, N particles, volume V, and temperature T. Assuming the defects do not interact, the total free energy F_{tot} of a crystal containing N_{S_L} and N_{L_S} antisite defects of type S_L and L_S, respectively, can be written as

$$F_{tot}(M,V,N_{S_L},N_{L_S}) = Mf_0(\rho_M) + N_{S_L}f_{S_L}(\rho_M) + N_{L_S}f_{L_S}(\rho_M) + F_c(M,N_{S_L},N_{L_S}), \quad (1)$$

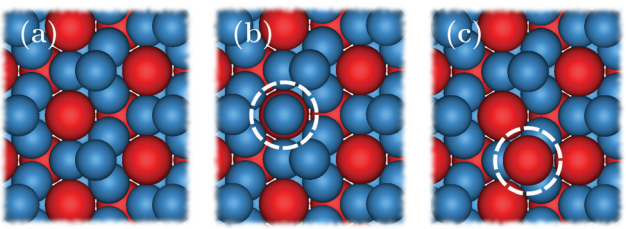

Fig. 1 (a) Ideal $MgZn_2$ structure. (b) S_L antisite defect where a small particle occupies a large-particle lattice site. (c) L_S antisite defect where a large particle occupies a small-particle lattice site.

with $\rho_M \equiv M/V$, $f_0(\rho_M)$ the free energy per particle of the defect-free crystal, and f_{S_L} (f_{L_S}) the change in free energy upon creating a single S_L (L_S) defect at a specific lattice site. Additionally, F_c is the combinatorial free energy resulting from the entropy of distributing the defects over all possible locations in the lattice, and is given by

$$\beta F_c(M,N_{S_L},N_{L_S}) = -\ln\left(\frac{M_L!}{(M_L-N_{S_L})!N_{S_L}!}\frac{M_S!}{(M_S-N_{L_S})!N_{L_S}!}\right) \quad (2)$$

with $M_L = \frac{1}{3}M$ and $M_S = \frac{2}{3}M$ the number of large-particle and small-particle lattice sites, respectively, and $\beta = 1/k_BT$ with k_B Boltzmann's constant. Note that we ignore the possibility of defects other than antisite defects (such as vacancies or interstitials), as these are known to be extremely rare in hard-sphere crystals.[33,34]

The free energy per particle of the defect-free crystal can be obtained for any given density ρ_M using

$$f_0(\rho_M) = f_0(\rho_M^r) + \int_{\rho_M^r}^{\rho_M}\frac{P_0(\rho_M')}{(\rho_M')^2}d\rho_M', \quad (3)$$

where $P_0(\rho_M)$ is the pressure, which we measure in standard event-driven molecular dynamics (EDMD) simulations.[36,37] Additionally, $f_0(\rho_M^r)$ is the Helmholtz free energy per particle at a given reference density of lattice sites ρ_M^r. For the Laves and FCC phases, reference free energies can be found in ref. 8 and 38 respectively.

We calculate f_{S_L} and f_{L_S} using Monte Carlo simulations in the canonical ensemble. In addition to standard Monte Carlo moves, we allow a single particle to fluctuate in size. We start off by initializing an ideal $MgZn_2$ crystal, and assign all particles to their corresponding lattice site. In order to prevent the spontaneous creation of additional defects, we confine the particles to their Wigner–Seitz cell by rejecting any particle move that will cause the center-of-mass of the particle to be closer to any other lattice point than its own.[39,40] This allows us to measure the free energy of a single antisite defect at a specific lattice site in a defect-free environment. Importantly, restricting the particles to their Wigner–Seitz cells has a minimal effect on the accessible phase space, mainly preventing the formation of additional interstitial-vacancy pairs. As shown in the ESI,† this has no measurable effect on the equation of state, and hence negligible effect on the free energy.

Focusing first on the S_L-defect, we allow a single large particle in the crystal to fluctuate in size during the simulation. This allows us to measure the change in free energy associated with changing the size of this specific particle. The free-energy difference $\Delta F(\sigma_a,\sigma_L)$ between a crystal with a particle of actual size σ_a and its nominal size σ_L at a specific lattice site is directly related to the probability $P(\sigma_a)$ of observing that size in the simulation:[33]

$$\Delta F(\sigma_a,\sigma_L) = F(\sigma_a) - F(\sigma_L) = k_BT\ln\left[\frac{P(\sigma_L)}{P(\sigma_a)}\right], \quad (4)$$

as plotted in Fig. 2(a). The free-energy cost of creating a single S_L-defect is then $f_{S_L} = \Delta F(\sigma_S,\sigma_L)$. Note that in order to ensure

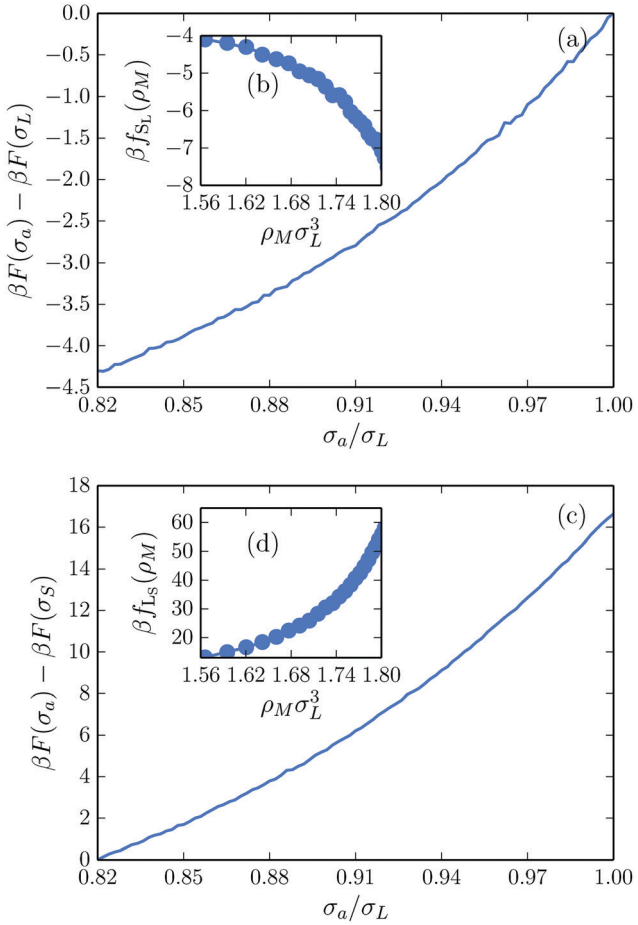

Fig. 2 Defect free energies associated with creating an antisite defect at (a and b) a large-particle lattice site and (c and d) a small-particle lattice site. (a) The free-energy difference associated with shrinking a single large particle to a size σ_a, at a density of $\rho_M{\sigma_L}^3 = 1.62$. (b) The defect free energy f_{S_L} as a function of the density ρ_M. (c) The free-energy difference associated with growing a single small particle to a size σ_a, at a density of $\rho_M{\sigma_L}^3 = 1.62$. (d) The defect free energy f_{L_S} as a function of the density ρ_M.

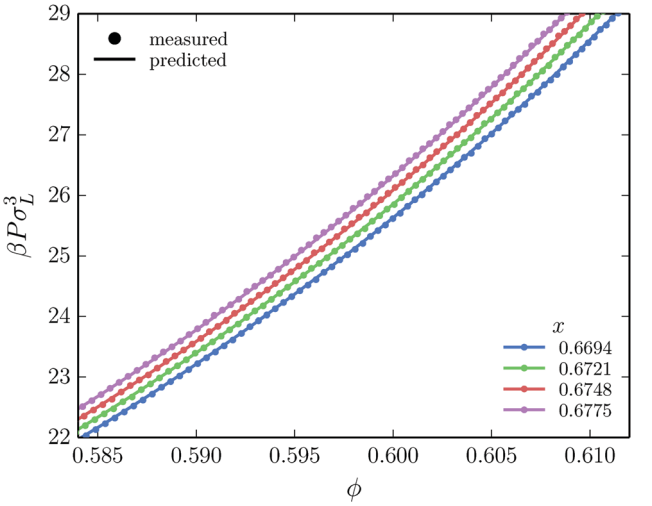

Fig. 3 Comparison of the pressure P as measured in EDMD simulations (markers) and as obtained from the free energy (lines). Different colors correspond to different concentrations of S_L-defects, which change the composition of the Laves phase x. Note that the volume fraction on the x-axis is given by $\phi = \frac{N\pi}{6V}{\sigma_L}^3[(1-x)+xq^3]$, with $q = 0.82$ the size ratio, N the number of particles, V the volume, and σ_L the diameter of the large spheres.

proper sampling of all possible sizes of the particle we make use of the Wang-Landau biasing method.[41]

We can extract f_{S_L} for a range of densities, as summarized in Fig. 2(b). For the L_S-defect, we repeat the same process but allow a small particle to fluctuate in size, with the results plotted in Fig. 2(c) and (d). It should be noted that the small particles in the $MgZn_2$ lattice appear in two different local environments, which in principle correspond to different free-energy costs f_{L_S}. However, since our calculations show that f_{L_S} is nearly identical for the two local environments, we ignore this distinction here.

As one might expect, the free-energy cost of shrinking a large particle is negative, while the cost of growing a small particle is positive: the pressure of the surrounding particles favors the shrinking of any particle in the crystal. Moreover, the cost of creating an L_S-defect is much higher than the gain of creating an S_L-defect, suggesting that simply swapping two particles in the crystal is not a favorable way to create defects. However, introducing excess S_L-defects has the potential to significantly lower the crystal free energy.

Using eqn (1), we can now calculate the full free energy of a crystal at a given density and composition, containing an arbitrary number of S_L- and L_S-defects. Moreover, we can calculate the pressure $P = -(\partial F_{tot}/\partial V)_{N,T}$ (at constant defect concentration) at each state point, giving us access to the Gibbs free energy $G = F + PV$ as well. In Fig. 3, we compare the pressure of defected $MgZn_2$ crystals, as derived from our expression for the free energy of the binary crystal phase, to the pressure as measured directly using event-driven molecular dynamics (EDMD) simulations,[42] for different concentrations of S_L antisite defects. Recall that in the expression for the free energy, we made the assumption that the defects do not interact. Clearly, we observe excellent agreement between the two approaches, justifying our assumption of non-interacting defects.

In addition to the antisite defects in the $MgZn_2$ crystal, it is also possible that "substitutional" defects are present in the FCC crystals. Specifically, as the system is by definition a mixture of large and small particles, it is possible for the FCC crystal of the large particles to include substitutional defects where a small particle replaces a large particle. Similar defects occur in the FCC crystal of small particles. The method we use to determine the free energy of the FCC crystals with these substitutional defects is analogous to the method used for $MgZn_2$ Laves phase (see the ESI† for more details).

3 Phase behavior with antisite defects

We now turn our attention to the effects of antisite defects on the phase diagram of hard-sphere mixtures. To predict the phase transitions in the system, we combine the free energies calculated for the defected crystals with the free energy of the fluid (taken from ref. 43). Phase coexistences are determined

using common-tangent constructions in the (x, g) plane, where $x = N_S/N$ is the composition and $g = \beta G/N$ is the Gibbs free energy per particle. Interestingly, we find that including antisite defects in our calculations significantly shifts the composition of the Laves phase coexisting with the fluid. As an example, we plot in Fig. 4 the common-tangent construction with and without defects for a fixed pressure $\beta P\sigma_L^3 = 23.3$. In the absence of defects, we find (black dotted line) a coexistence between a perfect crystal $x = 2/3$ and a binary fluid. However, taking into account the antisite defects (green dashed line), the fluid coexists with a strongly defected Laves phase, at composition $x = 0.672$. This shift in composition corresponds to a substantial net concentration of S_L-defects: around 1.6% of the large-particle lattice sites are taken up by small particles. Note that our calculations show that in all cases, the concentration of L_S-defects is negligible (see ESI†), and hence we ignore these defects when calculating the phase diagram.

Extending this approach to different pressures, and also considering substitutional defects in the FCC phases, we map out the revised phase diagram shown in Fig. 5(a), and provide a zoom-in of the Laves phase region in Fig. 5(b). As expected, allowing for defects expands the region of stability for the Laves phase from a single line at composition $x = 2/3$[7,8] to a narrow but finite region. What was not expected, however, is that at all pressures investigated this full region lies at composition greater than $x = 2/3$. In other words, the pure Laves phase is not stable at its "ideal" composition. While the shift in composition shown in Fig. 5(b) may appear to be small, it should be noted that the maximum shift (to $x \approx 0.6733$) corresponds to a full 2.0% of the large particles being substituted by small particles. This defect concentration is orders of magnitude higher than typical vacancy and interstitial concentrations in single-component hard-sphere crystals.[33,34] Aside from high S_L-defect concentrations, our phase diagram exhibits another interesting feature. For the fluid-Laves region our updated phase diagram reveals that at low pressures the S_L-defect concentration increases with pressure (as indicated by the increasing composition x). This is uncommon as usually the free-energy cost associated with the formation of defects increases strongly with pressure, resulting in lower defect concentrations.[34]

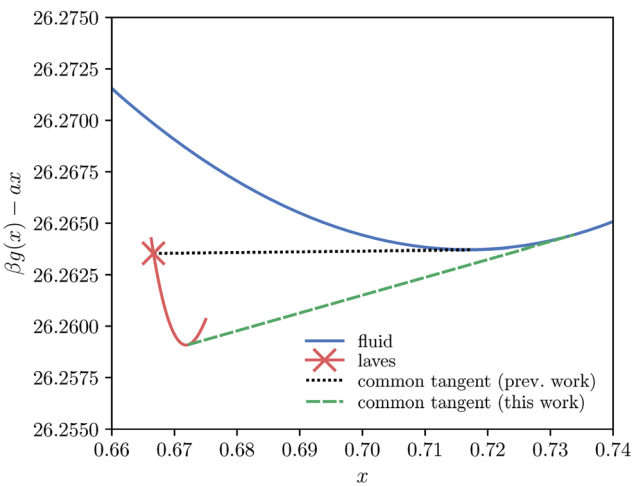

Fig. 4 Effect of taking antisite defects into account on the common-tangent construction between the fluid and Laves phase. Specifically, we plot the Gibbs free energy per particle $g = G/N$ as a function of the composition x at $\beta P\sigma_L^3 = 23.3$. A linear shift has been subtracted here to aid the visualization of the common-tangent construction. When only the ideal Laves composition ($x = 2/3$) is taken into consideration the common tangent between the fluid and Laves phase manifests itself as the horizontal line, as was used in previous work.[7,8] However, upon taking into consideration the Laves phase for a range of compositions it becomes clear that the common tangent is changed significantly. Note that in this plot the free-energy differences between different compositions appear a lot smaller than they are in reality due to the subtraction of a linear shift ax.

4 Estimating the impact of antisite defects

Lastly, we present a simple, approximate way to estimate the importance of these defects on a system where the defect-free phase diagram is known. In the following, we make the approximation that introducing antisite defects has no effect on the equation of state, and again assume that the defects do not interact. Under these assumptions, it can be shown (see ESI† for a full derivation) that the S_L-defect concentration is given by

$$\frac{N_{S_L}}{M_L} \simeq \exp\left(-\beta g_{S_L}\right), \tag{5}$$

where $g_{S_L} = f_{S_L} + \Delta\mu$ is the Gibbs free-energy cost of creating a defect at a specific lattice site, with $\Delta\mu = \mu_L - \mu_S$ the chemical potential difference between the two species. Applying this expression to defect-free phase coexistences, where the $\Delta\mu$ can be directly obtained from the slope of the (defect-free) common tangent, and f_{S_L} is taken from Monte Carlo simulations, we obtain an approximate phase diagram as shown by the red dashed lines in Fig. 5(c). Note that the common-tangent construction of the binary crystal structure typically involves phase coexistence with both a phase of lower composition (*e.g.* Laves + fcc_L) and with a phase of higher composition (*e.g.* Laves + fluid or Laves + fcc_S), each corresponding to their own value of $\Delta\mu$. This leads to a lower and upper bound for the equilibrium antisite defect concentration at a given pressure, and hence marks out the stability region of the defected crystal in the phase diagram.

As Fig. 5(c) shows, this first-order correction captures the essential traits of our "revised" phase diagram. Specifically, it predicts a similarly high concentration of defects, and captures the atypical defect concentration increasing with pressure in the fluid-Laves region. However, it still requires the measurement of f_{S_L} in simulations, and hence a significant additional effort when calculating the phase diagram. To this end, we try an even simpler approximation, where f_{S_L} is determined using cell theory. Specifically, we calculate for each particle the free volume that they can access when they are restricted to their own Wigner–Seitz cell in an otherwise perfect, static crystal. In this approximation, we can write the partition function as a product of volumes

$$Z = \prod_{i=1}^{N} \frac{v_i}{\Lambda^3} \tag{6}$$

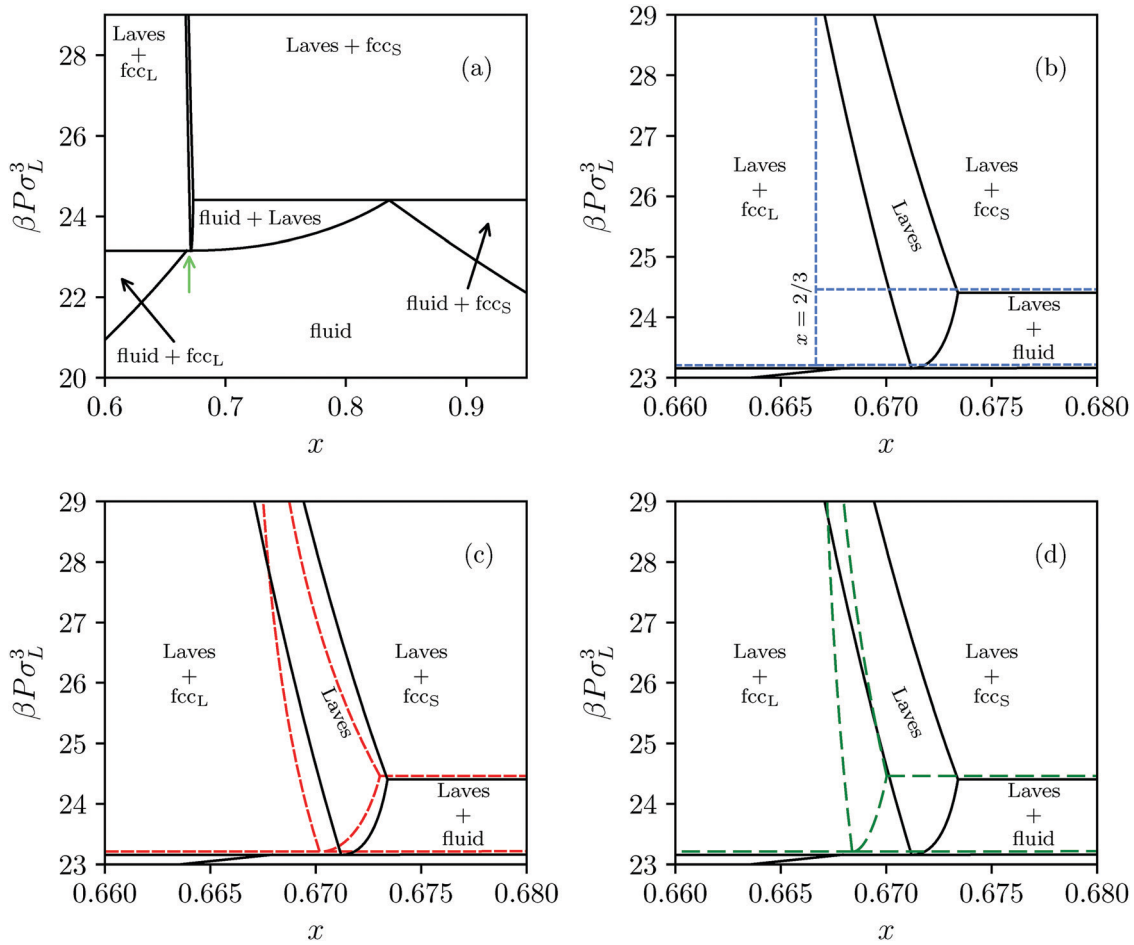

Fig. 5 (a) Revisited phase diagram for a binary hard-sphere mixture with a size ratio of $q = 0.82$ upon taking defects into account in both the Laves phase and FCC phases. (b–d) Zoomed-in section on the Laves phase region, where we compare different approximations (colored lines) with the revisited phase diagram (black lines). (b) The dashed blue lines correspond to the defect-free phase diagram as calculated in ref. 7 and 8. (c) The dashed red lines are obtained by using the approximate method to take into account antisite defects, *i.e.* by using eqn (5), and by taking f_{S_L} from Monte Carlo simulations. (d) The dashed green lines are again obtained by using eqn (5), but now taking f_{S_L} from cell theory. Note that there is an extremely small Laves phase + fluid region at the tip of the green arrow in (a) that is not visible on either of the pressure scales displayed here, as the pressure range of the region is $\beta\Delta P\sigma_L^3 = 0.002$.[31]

with Λ the De Broglie wavelength and v_i the free volume of a particle i, which we determine numerically by using Monte Carlo integration. Note that here, as in the rest of the paper, and without loss of generality, we choose the de Broglie wavelength to be the same for both species of particle. The defect free energy f_{S_L} associated with an S_L-defect is given by

$$\beta f_{S_L} = \sum_{i=1}^{N} \ln\left(\frac{v_i^0}{v_i^{S_L}}\right), \tag{7}$$

where $v_i^{S_L}$ and v_i^0 are the free volume of a particle i in a system with and without a S_L-defect, respectively. Using this mean-field defect free energy in connection with the approximation made in eqn (5), one can test the qualitative importance of antisite or substitutional defects on a phase transition. As shown in Fig. 5(d), while somewhat less accurate, this approach correctly captures the order of magnitude of the defect concentration and the topology of the phase diagram. Hence, this is a quick, computationally inexpensive recipe to check whether antisite defects are important in a known phase diagram.

5 Discussion and conclusions

In conclusion, we have shown that the equilibrium Laves phase in binary hard-sphere mixtures of size ratio $q = 0.82$ contains an extraordinarily high concentration of antisite defects. In fact, we find stable regions where up to 2% of the large-particle lattice sites are occupied by a small particle. This defect concentration is orders of magnitude higher than the vacancy and interstitial defect concentrations found in single-component hard-sphere crystals.[33,34] We expect these defects to play an important role for all size ratios for which the Laves phase is stable.

Our results highlight the need to carefully consider possible defects when predicting colloidal phase behavior, and in particular stress the need to consider non-stoichiometric perturbations of binary crystals. Clearly, the commonly made assumption in the calculation of phase diagrams that the crystal composition is ideal is not valid here. To date, these types of defects have not been considered in any of the binary hard-sphere crystal studies,[3–8,31] nor in any colloidal binary phase diagram studies that we are aware of. While we have focused here only on the Laves phase and

FCC crystals, we like to stress that the assumption of ideal crystal composition has also been made for the calculation of phase diagrams of binary hard spheres which show regions of stability of *e.g.* $NaZn_{13}$, AlB_2. As these crystals appear at more extreme size ratios, it might even be necessary to consider defects in which multiple small spheres take up the space of a single large sphere.

We presented a simple theoretical method to determine whether such defects are important for any predicted phase coexistence. This simple approach captured the essential traits of the ''updated'' phase diagram with little computational effort. This method is an excellent starting point for future studies of antisite defects in binary crystals.

Furthermore, our results highlight some striking similarities between colloids and atoms. Namely, we find the Laves phase to be thermodynamically stable for quite a broad range of composition – just like in atomic binary crystals, where the composition can be tuned through the incorporation of stoichiometric defects.[44–46] Hence, binary mixtures of colloids do not only provide an interesting model system of ''big atoms''[47,48] to study interstitial and substitutional solid solutions,[16–23,49–51] but also to study alloying in binary crystals.

Intriguingly, we find that the hard-sphere Laves phase is never thermodynamically stable at its ideal composition. This should be an important consideration in both experimental and computational attempts to study the nucleation of these crystals.[52–55] Lastly, much of the research on the Laves phases in colloidal crystals has been motivated by the possibility of a complete photonic band gap in the visible part of the spectrum, associated with the sublattices in the $MgCu_2$ crystal.[7,32] The high concentration of antisite defects we have found in the Laves phase with the $MgZn_2$ structure, is also very likely to play an important role in the other, metastable Laves phases with the $MgCu_2$ and $MgNi_2$ structures. Hence, high defect concentrations may affect the photonic band gap of the metastable $MgCu_2$ Laves phase, as it is well known that already low concentrations of defects can deteriorate the performance of band-gap materials. As these defects are an inherent part of the crystal phase behavior, removing them may be a considerable challenge.

Conflicts of interest

There are no conflicts to declare.

Acknowledgements

We acknowledge funding from the Dutch Sector Plan Physics and Chemistry. We thank Michiel Hermes and Alfons van Blaaderen for many useful discussions.

References

1 R. J. D. Tilley, *Defects in solids*, Wiley, New York, 2008.
2 B. Meyer, D. Hofmann, J. Niklas and J.-M. Spaeth, *Phys. Rev. B*, 1987, **36**, 1332.
3 M. D. Eldridge, P. A. Madden and D. Frenkel, *Nature*, 1993, **365**, 35.
4 M. D. Eldridge, P. A. Madden and D. Frenkel, *Mol. Phys.*, 1993, **79**, 105–120.
5 M. D. Eldridge, P. A. Madden, P. N. Pusey and P. Bartlett, *Mol. Phys.*, 1995, **84**, 395–420.
6 E. Trizac, M. D. Eldridge and P. A. Madden, *Mol. Phys.*, 1997, **90**, 675–678.
7 A.-P. Hynninen, J. H. J. Thijssen, E. C. M. Vermolen, M. Dijkstra and A. van Blaaderen, *Nat. Mater.*, 2007, **6**, 202.
8 A.-P. Hynninen, L. Filion and M. Dijkstra, *J. Chem. Phys.*, 2009, **131**, 064902.
9 T. Biben and J.-P. Hansen, *Phys. Rev. Lett.*, 1991, **66**, 2215.
10 M. Dijkstra, R. van Roij and R. Evans, *Phys. Rev. Lett.*, 1998, **81**, 2268.
11 M. Dijkstra, R. van Roij and R. Evans, *Phys. Rev. E*, 1999, **59**, 5744.
12 M. Dijkstra, R. van Roij and R. Evans, *Phys. Rev. Lett.*, 1999, **82**, 117.
13 A. D. Dinsmore, A. G. Yodh and D. J. Pine, *Phys. Rev. E*, 1995, **52**, 4045.
14 A. Imhof and J. K. G. Dhont, *Phys. Rev. Lett.*, 1995, **75**, 1662.
15 J. L. Barrat, M. Baus and J. P. Hansen, *Phys. Rev. Lett.*, 1986, **56**, 1063.
16 J. L. Barrat, M. Baus and J. P. Hansen, *J. Phys. C: Solid State Phys.*, 1987, **20**, 1413.
17 W. G. T. Kranendonk and D. Frenkel, *J. Phys.: Condens. Matter*, 1989, **1**, 7735.
18 D. A. Kofke, *Mol. Simul.*, 1991, **7**, 285–302.
19 W. G. T. Kranendonk and D. Frenkel, *Mol. Phys.*, 1991, **72**, 699–713.
20 W. G. T. Kranendonk and D. Frenkel, *Mol. Phys.*, 1991, **72**, 679–697.
21 X. Cottin and P. A. Monson, *J. Chem. Phys.*, 1993, **99**, 8914–8921.
22 L. Filion, M. Hermes, R. Ni, E. C. M. Vermolen, A. Kuijk, C. G. Christova, J. C. P. Stiefelhagen, T. Vissers, A. van Blaaderen and M. Dijkstra, *Phys. Rev. Lett.*, 2011, **107**, 168302.
23 I. Rios de Anda, F. Turci, R. P. Sear and C. P. Royall, *J. Chem. Phys.*, 2017, **147**, 124504.
24 P. Bartlett, R. H. Ottewill and P. N. Pusey, *J. Chem. Phys.*, 1990, **93**, 1299–1312.
25 P. Bartlett, R. H. Ottewill and P. N. Pusey, *Phys. Rev. Lett.*, 1992, **68**, 3801.
26 M. D. Eldridge, P. A. Madden and D. Frenkel, *Mol. Phys.*, 1993, **80**, 987–995.
27 X. Cottin and P. A. Monson, *J. Chem. Phys.*, 1995, **102**, 3354–3360.
28 N. Hunt, R. Jardine and P. Bartlett, *Phys. Rev. E*, 2000, **62**, 900.
29 A. B. Schofield, P. N. Pusey and P. Radcliffe, *Phys. Rev. E*, 2005, **72**, 31407.
30 S. R. Ganagalla and S. N. Punnathanam, *J. Chem. Phys.*, 2013, **138**, 174503.
31 T. Dasgupta and M. Dijkstra, *Soft Matter*, 2018, **14**, 2465.
32 E. C. M. Vermolen, J. H. J. Thijssen, A. Moroz, M. Megens and A. van Blaaderen, *Opt. Express*, 2009, **17**, 6952–6961.
33 S. Pronk and D. Frenkel, *J. Phys. Chem. B*, 2001, **105**, 6722–6727.
34 C. H. Bennett and B. J. Alder, *J. Chem. Phys.*, 1971, **54**, 4796–4808.
35 S. Pronk and D. Frenkel, *J. Chem. Phys.*, 2004, **120**, 6764–6768.

36 B. J. Alder and T. E. Wainwright, *J. Chem. Phys.*, 1959, **31**, 459–466.
37 M. P. Allen, D. Frenkel and J. Talbot, *Comput. Phys. Rep.*, 1989, **9**, 301–353.
38 J. M. Polson, E. Trizac, S. Pronk and D. Frenkel, *J. Chem. Phys.*, 2000, **112**, 5339–5342.
39 B. van der Meer, M. Dijkstra and L. Filion, *J. Chem. Phys.*, 2017, **146**, 244905.
40 B. van der Meer, R. van Damme, M. Dijkstra, F. Smallenburg and L. Filion, *Phys. Rev. Lett.*, 2018, **121**, 258001.
41 F. Wang and D. P. Landau, *Phys. Rev. Lett.*, 2001, **86**, 2050.
42 D. C. Rapaport, R. L. Blumberg, S. R. McKay and W. Christian, *et al.*, *Comput. Phys.*, 1996, **10**, 456.
43 G. A. Mansoori, N. F. Carnahan, K. E. Starling and T. W. Leland Jr, *J. Chem. Phys.*, 1971, **54**, 1523–1525.
44 D. J. Thoma and J. H. Perepezko, *J. Alloys Compd.*, 1995, **224**, 330–341.
45 J. H. Zhu and C. T. Liu, *Acta Mater.*, 2000, **48**, 2339–2347.
46 F. Stein, D. Jiang, M. Palm, G. Sauthoff, D. Grüner and G. Kreiner, *Intermetallics*, 2008, **16**, 785–792.
47 D. Frenkel, *Science*, 2002, **296**, 65–66.
48 W. Poon, *Science*, 2004, **304**, 830–831.
49 J. Tauber, R. Higler and J. Sprakel, *Proc. Natl. Acad. Sci. U. S. A.*, 2016, **113**, 13660–13665.
50 R. Higler and J. Sprakel, *Sci. Rep.*, 2017, **7**, 12634.
51 B. van der Meer, E. Lathouwers, F. Smallenburg and L. Filion, *J. Chem. Phys.*, 2017, **147**, 234903.
52 P. K. Bommineni, M. Klement and M. Engel, 2019, arXiv preprint, arXiv:1912.06251.
53 T. Dasgupta, G. M. Coli and M. Dijkstra, 2019, arXiv preprint, arXiv:1906.10680, to be published in ACS Nano.
54 D. Wang, T. Dasgupta, E. B. van der Wee, D. Zanaga, T. Altantzis, Y. Wu, G. M. Coli, C. B. Murray, S. Bals, M. Dijkstra, *et al.*, 2019, arXiv preprint, arXiv:1906.10088.
55 N. Schaertl, D. Botin, T. Palberg and E. Bartsch, *Soft Matter*, 2018, **14**, 5130–5139.